SPACE CHARGES IN MATERIAL SCIENCE

Gerhard Herzog
Institut für Chemische Technologie Anorganischer Stoffe
Technische Universität Graz, Austria

INVITED PAPER
23rd International Conference on Microelectronics, MIEL'95
31st Symposium on Devices and Materials, SD'95
September 27.-September 29., 1995, Terme Čatež, Slovenia

Key words: material science, space charges, electric charges, interfacial phenomena, liquid materials, contact regions, semiconductor materials, electroceramic materials, electrolytic materials, practical applications, photoactive materials, semiconductor interfaces, dry solar cells, electrolytical solar cells, solutions, Debye-Hueckel theory, dielectric media, MOS transistors, varistor effect, PTC effect, Positive Temperature Coefficient effect, passive layers, photo catalysis

Abstract: Whenever two different liquid and/or solid materials are brought into contact with each other, interfacial phenomena occur. Space charges, built up in the contact region or interface are the key to their understanding. In some electrical components or devices at all, space charges are intentionally used, but in many other cases they are undesired and must be eliminated. In an introductory review principles and applications of space charges in and at electrolytical (I), semiconducting (II) and electroceramic (III) materials are described. A special application of space charges are photo or solar devices (IV), which will finally be discussed.

The reason for including electrolytical systems is a historical one too, because the treatment of space charges by Debye and Hückel, aiming at chemical and electrical properties, was carried out a long time ago before solid contacts became interesting. However, the goal of their treatment is so general, that we can easily transfer and extend the basic ideas to nowadays modern materials and devices.

Prostorski naboji v znanosti o materialih

Ključne besede: znanost o materialih, naboji prostorski, naboji električni, pojavi vmesniški, materiali tekoči, področja stična, materiali polprevodniški, materiali elektrokeramični, materiali elektrolitični, aplikacije praktične, materiali fotoaktivni, področja stična polprevodnikov, celice sončne suhe, celice sončne elektrolitične, razstopine, Debye-Hueckel teorija, mediji dielektrični, MOS transistorji, efekt varistorski, PTC efekt koeficienta temperaturnega pozitivnega, plasti pasivne, kataliza foto

Povzetek: Kadarkoli stopita dve različni tekoči ali trdni snovi v kontakt, pride do površinskih pojavov. Prostorski naboji, ki se tvorijo v območju kontakta ali na površini, so ključ za razumevanje teh pojavov. V nekaterih elektronskih komponentah površinske naboje namenoma uporabljamo, drugje pa so nezaželjeni in se jih želimo znebiti. V prispevku na pregleden način podajamo osnove in opisujemo uporabo prostorskih nabojev v in na elektrolitičnih (I), polprevodniških (II) in elektrokeramičnih (III) materialih. Posebno področje uporabe prostorskih nabojev so foto, oz. sončne komponente (IV), o katerih bomo govorili na koncu.

Razlog, zakaj smo v ta prispevek vključili tudi elektrolitične sisteme, je deloma zgodovinski, saj sta prostorske naboje obravnavala že Debye in Hückel. Njiju so predvsem zanimale njihove kemične in električne lastnosti, čeprav je bilo njuno delo opravljeno preden so meje in stična področja med snovmi v trdnem stanju sploh postale aktualne. Kljub vsemu je njuna obravnava tako splošne narave, da jo lahko mirno prenesemo in razširimo na področje današnjih modernih materialov in komponent.

I. SPACE CHARGES WITHIN SOLUTIONS

Debye-Hückel theory

Any ensemble of localised or mobile electronic or ionic charge carriers in a dielectric medium builds up a charge distribution or space charge. Look at the simplest and most familiar case, i.e. ions in an electrolytical solution. Cations and anions are mobile because of thermal agitation in the dielectric material of water. They arrange themselves by the action of electrostatic forces until the minimum of free system energy is reached.

Ions in a solution don't order in a lattice structure, because their thermal energy is too high. As well they are hydrated with water dipoles, which break long range ordering. Looking, however, at nearest ion-ion distances, we observe a certain kind of order. Each hydrated cation is surrounded by an ion shell, which itself is on the average negatively charged. So we can speak of an ion cloud around the cation, which makes it heavy and sluggish, when it is forced to move in an electrical field. This cloud is also the reason why ions move with about the same velocity or mobility and show relaxation effects like dipoles.

The structure of the cloud is governed by electrostatic interactions between the hydrated ions and their thermal agitation. The cloud structure is necessarily centrosymmetric. All we have to do for a quantitative treatment is to solve the Poisson-Boltzmann equation, which is merely a combination of the electrostatic Poisson equation and a statistical Boltzmann expression for the charge density ρ (pair function):

$$\Delta\varphi \sim \rho$$

$$\sim \sum_i q_i c_i e^{-q_i\varphi/kT} \qquad (1)$$

A power series expansion and some abbreviations lead to the following simplified differential equation for the electrical potential φ in the neighbourhood of the central cation:

$$\Delta\varphi = \beta\varphi \qquad (2)$$

The parameter β contains the ionic charges q_i, the concentrations c_i, the temperature T and the dielectric constant of water ε. Solving equ. (2) to a first approximation one obtains for the electrostatic potential

$$\varphi(r) \sim \frac{1}{r} e^{-\sqrt{\beta}\, r} \qquad (3)$$

and for the charge density profile:

$$\rho(r) \sim -\frac{\beta}{r} e^{-\sqrt{\beta}\, r} \qquad (4)$$

As shown in fig.1 both the potential φ(r) and the space charge density ρ(r) behave exponentially /1/. The so-called Debye-radius $1/\sqrt{\beta}$ is a measure for their mean spatial extension. In other words, the central ion is screened by the ionic cloud to a more or less extent, depending mainly on the ionic carrier concentration or ionic strength. The higher the concentration the stronger is the screening and the thinner is the space charge around the central ion. The energy difference between the isolated and the screened central ion corresponds to the difference of the chemical potential of the cation and is therefore related to the activity coefficient. This concept is only valid for low-concentrated solutions.

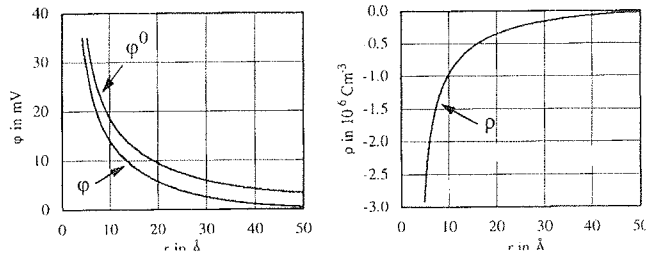

Fig.1: Potential and density profiles

Electrolytical space charge at a metal electrode

When a metal electrode is dipped into a solution and is external charged, it creates also an electrolytical space charge with a similar exponential behaviour of charge and potential profiles. Here traditionally the ionic arrangement is called diffuse double layer. Once again, with great ion concentrations the diffuse layer is relatively thin and what remains is a kind of surface instead of space charge. It is most probably mixed with adsorbed and oriented water dipoles.

Only when the metal is polarisable the contact can be biased externally, otherwise an electrochemical reac-

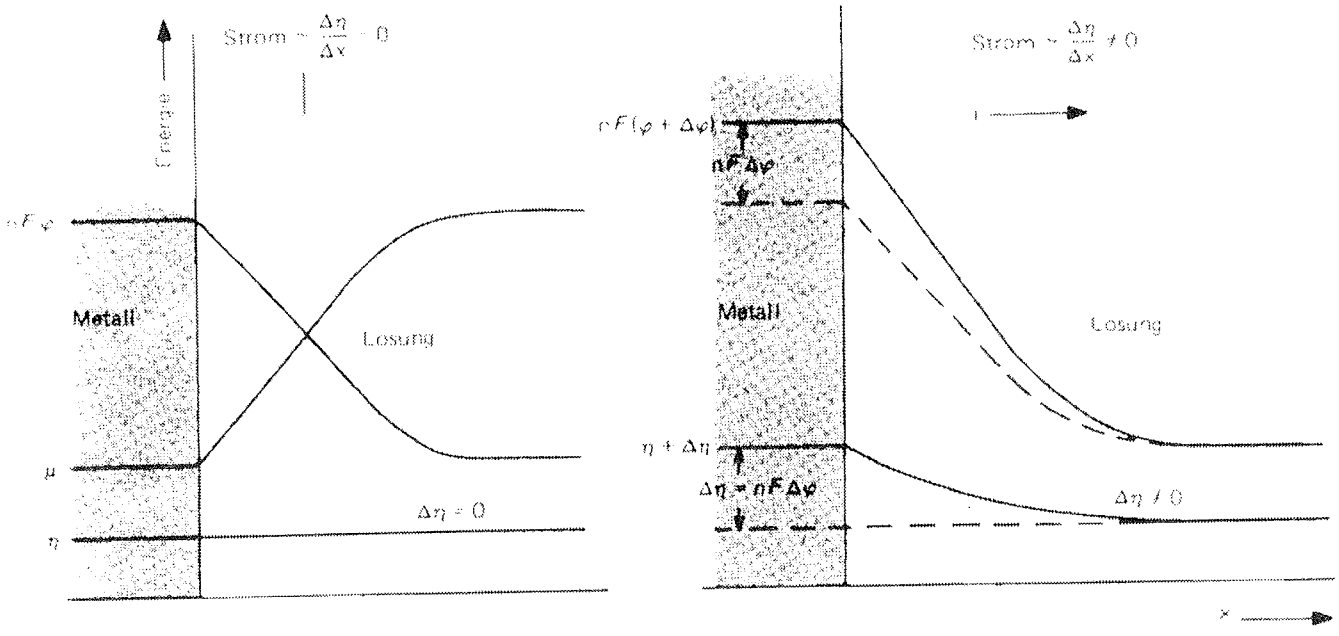

Fig. 2: Electrochemical equilibrium and non-equilibrium

tion proceeds. Equilibrium and non-equilibrium, described by the difference of the electrochemical potential η of exchangeable particles in both phases, is schematically shown in fig.2. In the situation $\Delta\eta \neq 0$, a faradaic current due to some reaction will flow /1/.

Measurement of electrolytical space charges

Spatial dependences of charges and potentials at interfaces cannot be measured directly. By electrical means we can only observe overall or statistically averaged

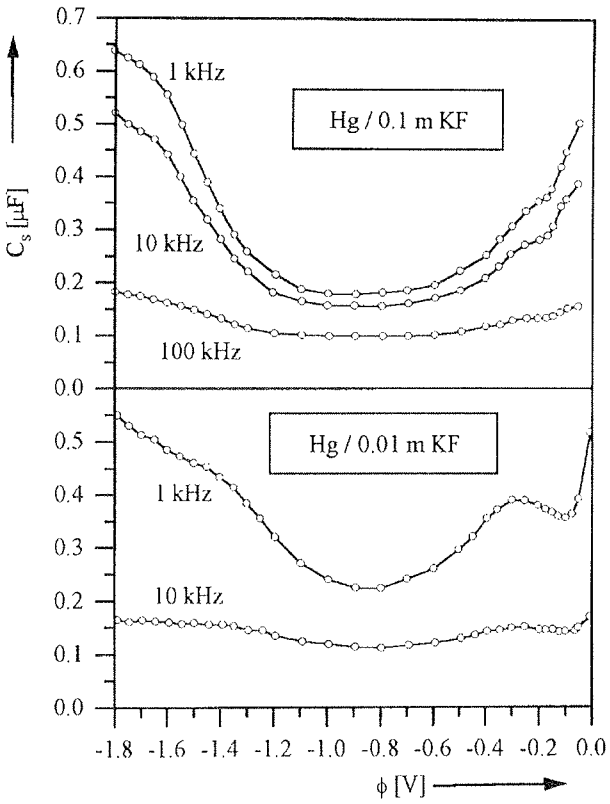

Fig. 3: The potential (vs. Hg/HgO) dependence of double-layer capacitance at 30 °C

properties as the integral or differential capacitance. As space charges at interfaces act like ensembles of dipoles the most convenient experimental method is impedance spectroscopy in the frequency or time domain. Both domains are interconnected via Fourier transformation. Physically most profitable results are obtained by capacitance/voltage dependences and relaxation time analysis. In the years 1975 to 1980 we especially studied contacts with metallic micro-electrodes. The experimental curves in fig. 3 show, that the differential capacitance vs. voltage behaves parabolic with superimposed humps /2/. When the parabola are ascribed to faradaic capacitances, the humps remain to be explained.

Explanation by an adsorption model

From our experimental studies a simple thermodynamical adsorption model for ions at metal contacts was claimed /3/. The basic assumption is an electrochemical equilibrium between dissolved ions A, free adsorption states B and adsorbed ions AB with a Langmuir-like concentration dependence. By differentiation of the adsorbed charge with respect to the electrical potential drop between the surface and the bulk phase an expression for the differential capacitance is obtained. Although in this model only one kind of ions is involved and adsorbed water dipoles as well as a diffuse layer were neglected, it gives a good approach of the observed capacitance/potential behaviour and predicts humps on both sides of zero potential quite easily (fig. 4).

$$\Delta\eta = \Delta\mu + e\Delta\varphi = 0 \tag{5}$$

$$\Delta\eta = -kT\,lnK + kT\,ln\frac{c_{AB}}{\left({}^{0}c_{AB} - c_{AB}\right)c_B} + e\Delta\varphi = 0 \tag{6}$$

$$c_{AB} = {}^{0}c_A \frac{1}{1 + \frac{1}{Kc_B} e^{e\Delta\varphi/kT}} \tag{7}$$

$$C = \frac{\partial e c_{AB}}{\partial\Delta\varphi} = \frac{e^2}{kT}\,{}^{0}c_A \frac{Kc_B e^{e\Delta\varphi/kT}}{\left(Kc_B + e^{e\Delta\varphi/kT}\right)^2} \tag{8}$$

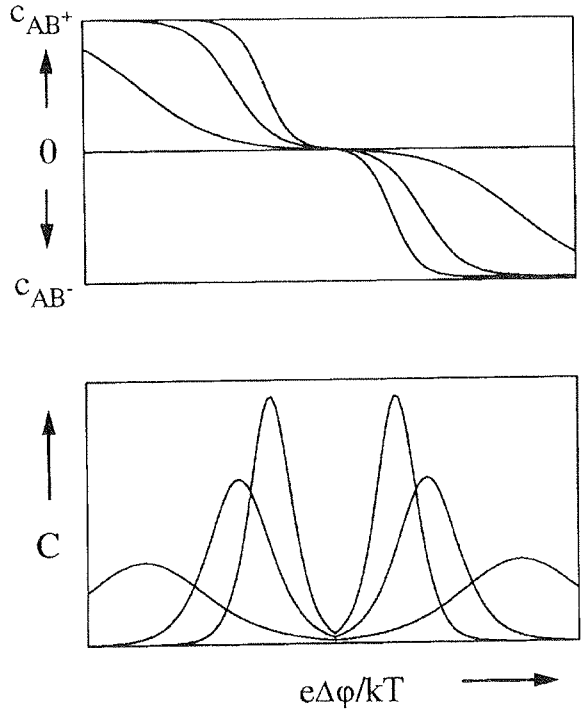

Fig. 4: Adsorbed ion density and differential capacity

Simulation of electrolytical space charges

Since the ab initio treatment of metal-electrolyte contacts is quite impossible, we tried to get more insight by a grand canonical Monte-Carlo simulation using the most simple potential functions for ion-ion and ion-metal interactions. The solution was simulated by hard sphere ions in a homogenous water dielectric, because ten years ago the application of soft potentials, allthough now available was too CPU time consuming.

According to the above mentioned adsorption model the chemical potential difference of the surface and the bulk phase of the solution must be calculated. The surface phase is enriched with ionic excess charges because of its contact with an externally charged wall. Since this can only be done in a grand canonical simulation, our Monte-Carlo program with Metropolis sampling was adapted to a grand canonical (μ,V,T) ensemble with variable ion number N. The simulation procedure consisted of the following steps /4/.

1. Movement of a random ion as in canonical simulation with an analogous exponential probability.
2. Stochastical decision if an ion is added or subtracted and continuation with step 3 or 4.
3. Ion addition at a random position in the system and acceptance probability with new ion number N. Continuation with step 1.
4. Ion subtraction using a randomly selected particle with a proper acceptance probability. Continuation with step 1.

In the following the transition probabilities p_{ij} are given. ΔU is the potential energy change of the whole particle configuration. The free parameter B contains the chemical excess potential μ' and the equilibrated particle number N' /5/:

$$p_{ij} = 1 \quad \text{for} \quad \frac{\Delta U}{kT} \leq 0$$
$$p_{ij} = e^{-\Delta U/kT} \quad \text{for} \quad \frac{\Delta U}{kT} > 0 \tag{9}$$

$$p_{ij} = 1 \quad \text{for} \quad \frac{1}{N} e^{B-\Delta U/kT} \geq 1$$
$$p_{ij} = \frac{1}{N} e^{B-\Delta U/kT} \quad \text{for} \quad \frac{1}{N} e^{B-\Delta U/kT} < 1 \tag{10}$$

$$p_{ij} = 1 \quad \text{for} \quad N e^{-B-\Delta U/kT} \geq 1$$
$$p_{ij} = N e^{-B-\Delta U/kT} \quad \text{for} \quad N e^{-B-\Delta U/kT} < 1 \tag{11}$$

$$B = \frac{\mu'}{kT} + \ln N' \tag{12}$$

After a simulation run with a given parameter B the excess potential or activity coefficient γ is found:

$$\gamma = e^{B-\ln N'} \tag{13}$$

The simulation procedure was proved by calculating the concentration dependence of the activity coefficient in comparison with the first and second Debye-Hückel approximations. For the simulation of metal-electrolyte contacts the metal-ion interaction was modeled by the effective potential

$$V = \frac{PeZe}{4\pi\varepsilon_0 x} \tag{14}$$

The external potential, equivalent to the potential drop $\Delta\varphi$ between the metal and the solution, is established during simulation by the ionic density profiles and is varied implicitely via the parameter P.

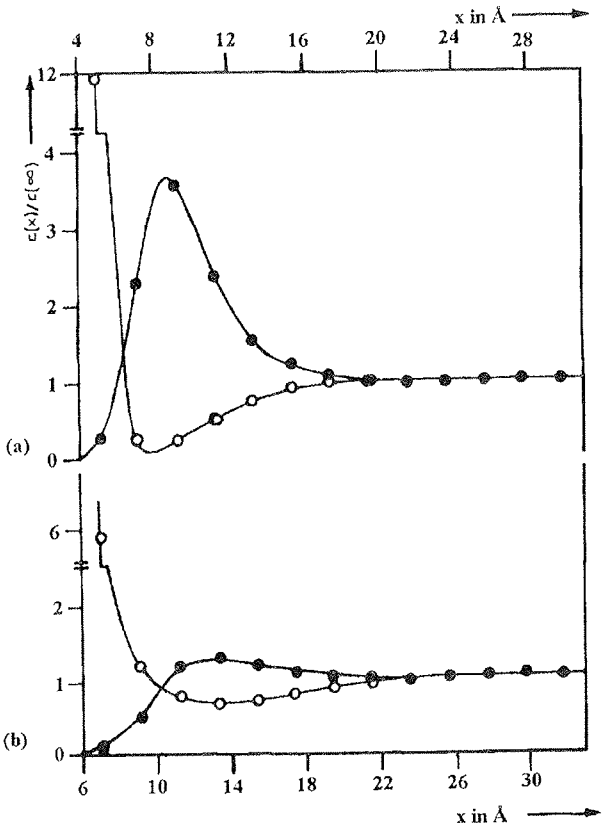

Fig. 5: Simulated density profiles of anions (o) and cations (•) with metal charge Pe at x = 0 and metal boundaries at x = 4 (a) and x = 6 Å (b)

Results of simulation

Two typical examples of profiles are shown in fig. 5. Both anions and cations are accumulated in the surface phase of about 20 Å extension. From the difference of the total ion numbers N' the excess charge q is obtained. Comparing the system with a plate condenser, one is able to calculate by means of the Poisson equation the electrical potential drop at the metal-electrolyte contact:

$$\Delta\varphi = -\frac{q\bar{x}}{\varepsilon_0\varepsilon F} = -\frac{q}{\varepsilon_0\varepsilon}\int_{x=0}^{\infty}(c_+ - c_-)x\,dx \qquad (15)$$

The main goal, however, of this simulation work was to obtain charging curves from which by differentiation the differential capacitance is obtainable (fig. 6). At small potential drops the hard sphere system behaves like an ideal plate condenser. With increasing charge there is an increase of the differential capacitance as expected, but unfortunately because of missing CPU time we could not wait until a hump came out.

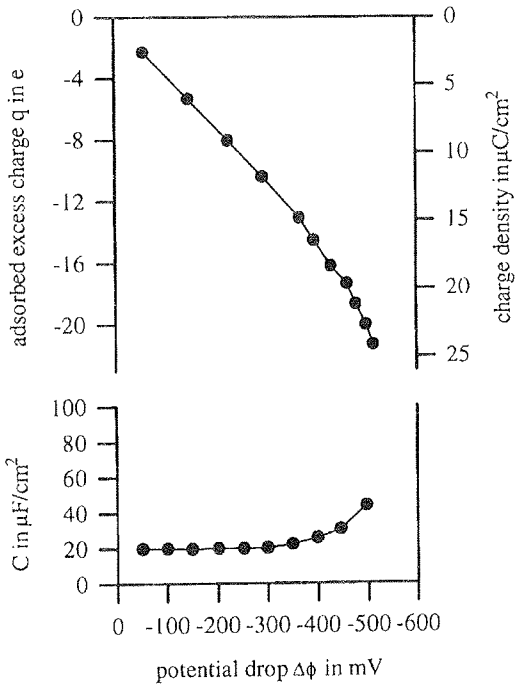

Fig. 6: Simulated charge density and capacity curves

Experiences from the study of electrolytical space charges

Before switching over to a discussion of some real and practically more important solid-solid contacts, let us summarise what we can learn just from electrolytical space charges.

- Space charges or double layers occur between two chemically different and eventually externally charged phases, when mobile ions or electron/holes are present.
- The charge and potential profiles are connected through the Poisson equation. They extend exponentially into the bulk phase, and look like double layers when the mobility of the charge carriers is high.
- Equilibrium is given by the balanced electrochemical potential within two phases being in contact, beyond equilibrium reactions with charge transfer will occur.
- In general, charge and potential profiles cannot be measured directly, only potential drops and capacitances with the help of plate condenser model. Charging and/or capacitance depend non-linearly on external bias.
- To interpret charging or capacitance curves potential models preferring either surface or diffuse profiles, have to be introduced but remain ambiguous.
- Computer simulations can support the interpretation of statistical properties as the capacitance, but they depend on proper atomic potentials.
- Generalisation to solid-solid interfaces is only a gradual step, bearing in mind that the mobility of charged species can be very different.

II. SPACE CHARGES IN AND AT SEMICONDUCTORS

As already mentioned, it is very instructive to discuss space charge phenomena with respect to their practical importance. So, some applications of semiconductor-electrolyte interfaces concern corrosion and photo processes, which can be desired or undesired.

When we dip a metal like Fe, Zn, Al, Si or Ti into a corrosive solution, the growing oxide layer behaves like a semiconductor because of unoxidised metal atoms. On the other hand the same will happen with Si in an O-containing atmosphere at high temperatures (see SiO_2 formation in MOS technology). Advanced formation of an intact layer lowers the rate of corrosion, which is very useful, although corrosion itself is not. The semiconducting properties of the oxide layer control the progress of the corrosion via transport of mass and charge. Of course any external bias can enlarge or prevent this process by the formation of space charges at both sides of the interface, one within the semiconductor and one within the electrolyte. In the following we don't take care of the latter and confine ourselves to the first.

Space charges in semiconductors

When a semiconductor is externally charged a space charge in the surface region is built up. From the solution of Poisson equation with FD statistics for mobile electrons or holes and neutrality condition, three different cases can be distinguished (fig. 7): Accumulation, depletion and inversion of majority carriers. For small surface charges the solution for potential and density

profiles is once more an exponential function of extension, the Debye-length now given by

$$L = \sqrt{\frac{\varepsilon\varepsilon_0 kT}{e^2(n+p)}} \qquad (16)$$

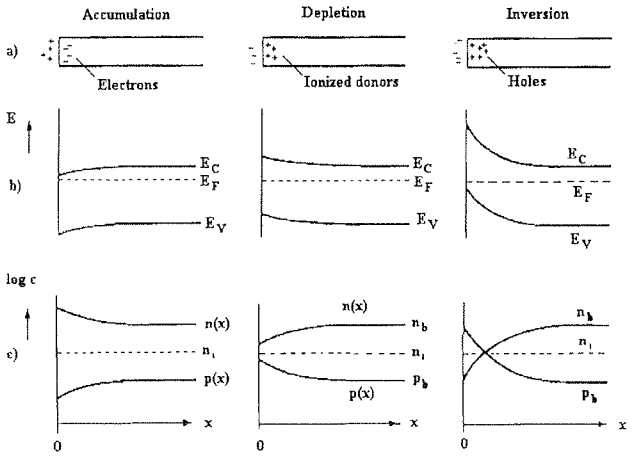

Fig. 7: Charge distribution (a), electron energy (b) and carrier concentration (c) of space charge layers in n-semiconductors, taken from /6/

Following Schottky the depletion case can be treated with a separate approximation, if all donors are ionised and the charge density is merely given by the constant donor density N. From twofold integration the potential proftle (0<x<d) and the band bending φ_S at the surface (x = 0) is obtained

$$\varphi_s = \frac{eN}{2\varepsilon_0\varepsilon} d^2 \qquad (17)$$

As the total space charge within the region d is q=edN:

$$\varphi_s = \frac{q^2}{2\varepsilon_0\varepsilon Ne} \qquad (18)$$

and 1/C = dφ /dq, we obtain a very useful expression for determining donor densities from capacitance measurements:

$$\left(\frac{1}{C}\right)^2 = \frac{2}{2\varepsilon\varepsilon_0 Ne}\varphi_s \qquad (19)$$

There are a lot of applications of equ. (19), two of them are shown in fig. 8 and 9. They concern ZnO-crystal- and corroded Zn-electrolyte contacts to confirm semiconduction of the as-grown oxide layers /7/. We will return to the depletion case in the discussion of electroceramic components.

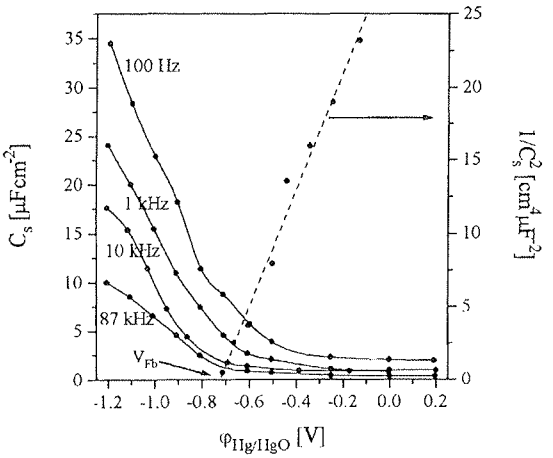

Fig. 8: Potential dependence of double layer capacitance C_S of ZnO - 0.1 M borax at various frequences

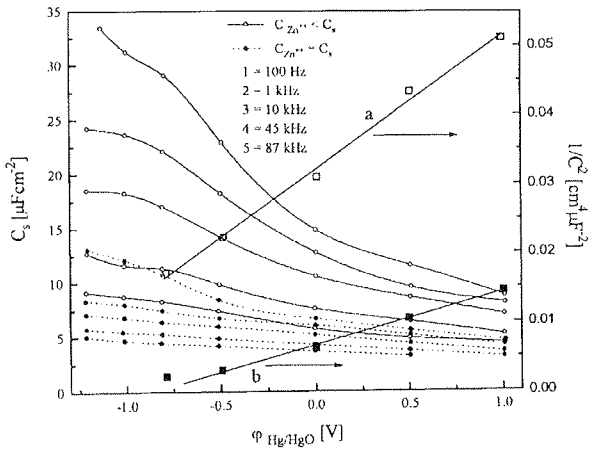

Fig. 9: Schottky plots of corroding Zn - 0.1 M borax without (a) and with (b) correction due to the electrolytical capacitance

The MOS transistor

Todays best-known and most important application of space charge theory is the MOS transistor, which operates under inversion condition. The transistor principally consists of a MOS capacitor, to which a gate voltage is applied, and of drain-source electrodes attached to the channel region to pick up the drain current (fig.10).

As can be seen from drain current/voltage curves for operation a certain minimum gate voltage the so-called threshold voltage is necessary. Inversion is established,

when the band bending φ_S is twice the difference of the Fermi and donor or acceptor energy ϕ. In this case the minority carrier density at the surface becomes as large as the majority carrier density in the bulk. The corresponding energy situation is outlined in fig. 11.

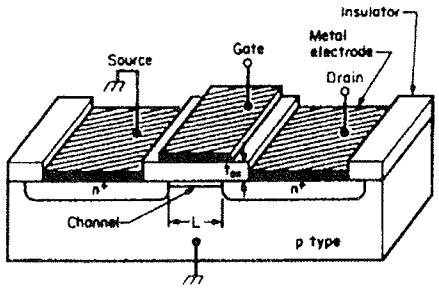

Fig. 10: n-channel MOS transistor, taken from /8/

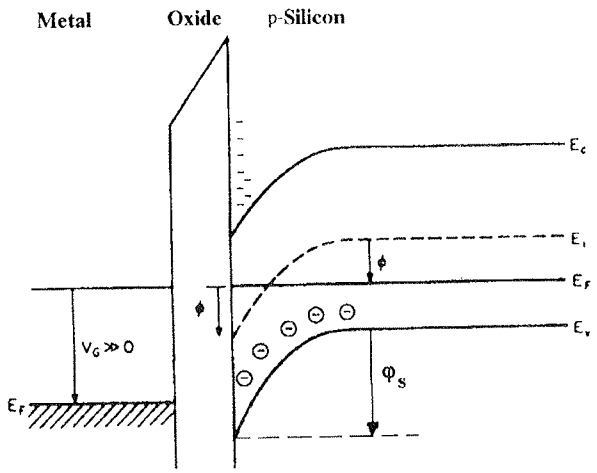

Fig. 11: Band bending in the case of inversion

ε_S is the dielectric constant of Si, N the acceptor density, C_0 is the oxide capacity and ϕ is the above defined energy difference. In the theory so far we have assumed an uniform substrate doping. But in a real MOS-device, the doping profile is far from uniformity. Impurity ions will be redistributed during thermal processes and ion implanted profiles are intentionally applied /9/ for a better design of devices (fig. 12).

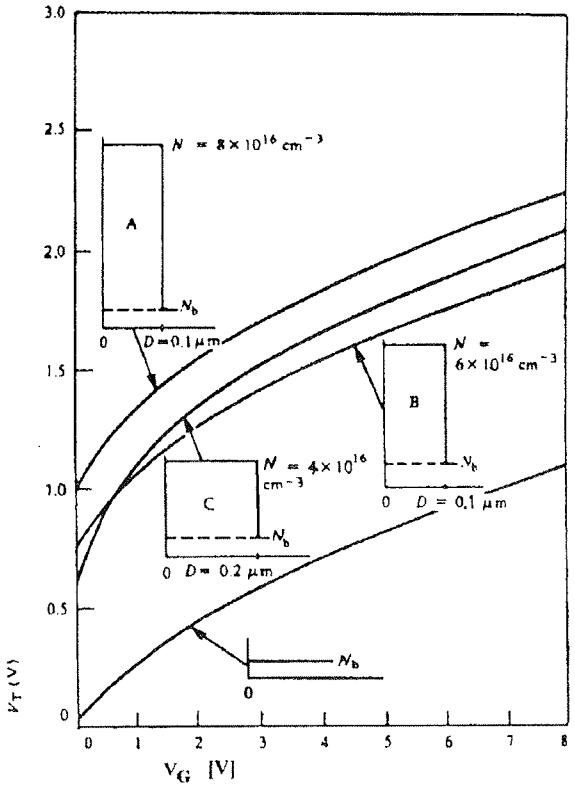

Fig. 12: Calculated treshold voltage for some cases of implantation, taken from /9/

Dielectric and charge balance considerations lead to the central expression for the treshold voltage of n-channels:

$$V_T = V_{Fb} + \frac{1}{C_0}\sqrt{2e\varepsilon_s\varepsilon_0 N(2\phi + V_G)} + 2\phi \qquad (19)$$

In the ideal case the flat band voltage $V_{Fb}=0$, otherwise V_{Fb} is determined by the difference of the work functions V_{MS} and the space charges located near the Si-SiO_2-boundary.

$$V_{Fb} = V_{MS} + \sum \frac{space\ charges}{C_0} \qquad (20)$$

MOS capacitance/voltage plots

As with metal-electrolyte contacts most instructive knowledge about space charges within MOS-structures are obtained from CV measurements (fig. 13). It is easily realized what is measured with such a setup. With negative gate bias p-type silicon is in accumulation and the capacitance (C) is simply that of a parallel plate condenser with SiO_2 as the dielectric (C_0). At a gate voltage V_G that is more positive than the flatband voltage (V_{FB}) depletion is established and creates a space charge capacitance in series. When the gate voltage exceeds the threshold voltage inversion is formed and then the total capacitance depends on the measuring frequency. If in the high frequency case the inversion layer cannot follow the AC field the total capacitance will be minimum (C_{min}) and stay constant with increasing gate voltage. Deep depletion is only observed with fast enough potential scan.

A simple analysis for the CV curves in the depletion and inversion region yields

$$\frac{C}{C_0} = \left(\sqrt{1+\frac{V_G}{V_0}}\right)^{-1} \qquad \left(V_0 = \frac{eN\varepsilon_s\varepsilon_0}{2C_0^2}\right) \qquad (21)$$

$$\frac{C_{min}}{C_0} = \left(\sqrt{1+\frac{V_T}{V_0}}\right)^{-1} \qquad (22)$$

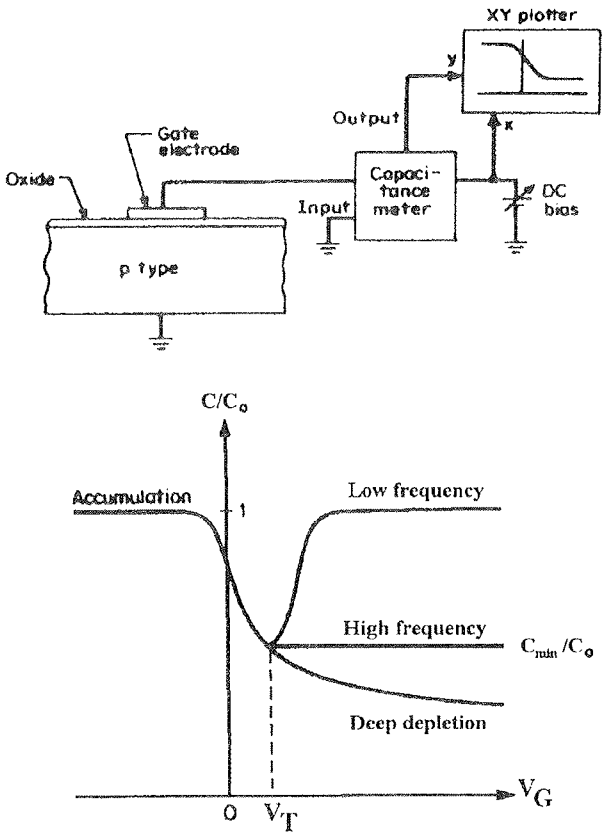

Fig. 13: CV setup and frequency dependent CV plots, taken from /8/

From CV plots implanted regions can be evaluated (fig. 14) /10,11/ and undesired space charges can be identified /12/. They must be minimised during the processing of devices. However, the structural mismatch between Si and SiO_2 is an intrinsic property /13/. In general one has four types of charges with the thermally grown oxide interface /14/,

1) fixed oxide charges,
2) mobile ionic charges,
3) interface states and
4) oxide trapped charges,

each of them causing characteristical shifts or other kinds of deviation.

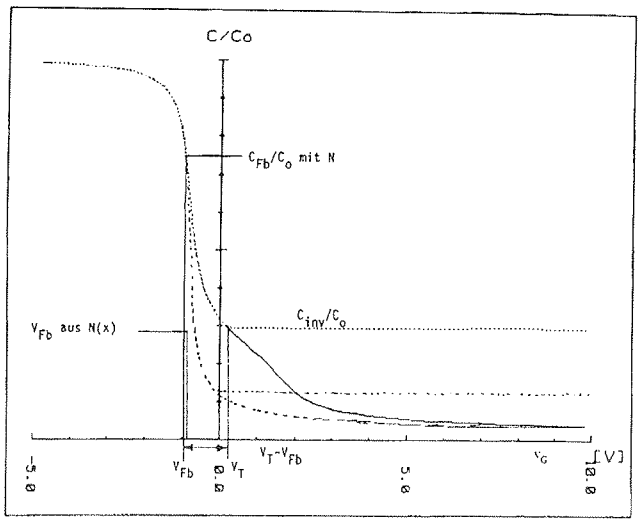

Fig. 14a: CV plots of implanted (upper curve) and native (lower curve) p-material

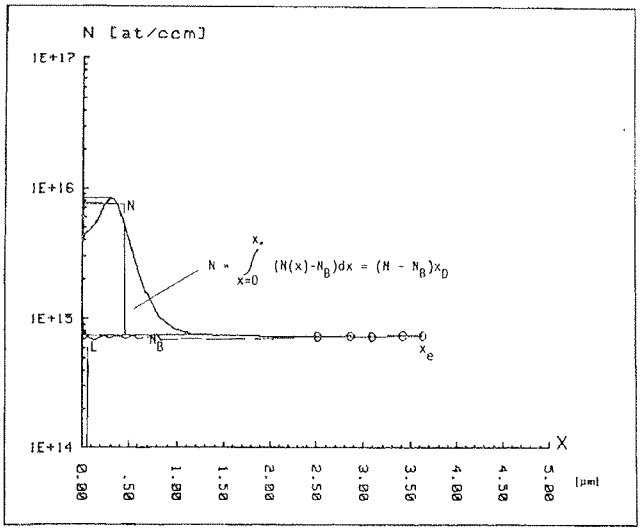

Fig. 14b: Evaluation of implanted profiles

III. SPACE CHARGES IN AND AT ELECTROCERAMIC MATERIALS

The key effects in electroceramic components as ZnO varistors and PTC's made of doped $BaTiO_3$ are most probably a crucial consequence of space charges at grain boundaries, and not of internal blocking layers or external electrode contacts. In a stochiometric composition both materials are insulators with band gaps of about 3 eV. By a proper doping of single crystals with aliovalent impurities both materials become n-semicon-

ducting, ZnO showing band and $BaTiO_3$ polaronic conduction. However, in a ceramic material up to a certain breakdown voltage ZnO and above the Curie temperature $BaTiO_3$ are insulators.

Double Schottky layers

What is desired in electroceramics? Good varistors should have a steep current increase at the breakdown voltage (especially for low-voltage protection) and PTC's should have a steep resistance increase at a certain temperature. Although both characteristics look very different, their underlying basic electrical phenomenon is quite the same. At grain boundaries inside the same ceramic material acceptor surface charges are assumed to be generated during processing, which themselves create space charges at each side of the boundary /15,16/. So a double Schottky depletion layer with an energy barrier is formed (fig.15).

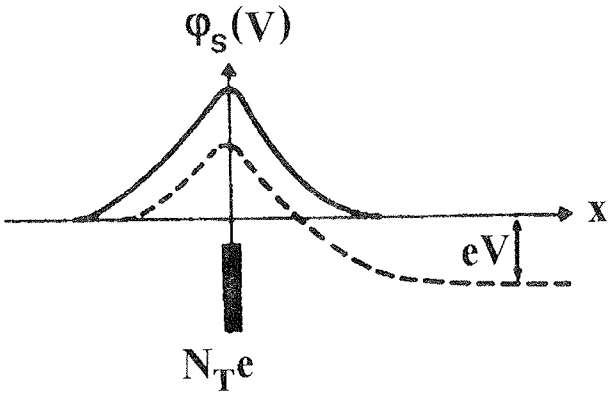

Fig.15: Energy barrier without and with external bias

According to equ. (18) the barrier height is proportional to the square of the surface trap density N_T at the boundary and inverse to the donor density N:

$$\varphi_s = \frac{N_T^2 e}{2\varepsilon_0 \varepsilon N} \tag{23}$$

As conduction electrons have to overcome the barrier (activation energy), the resisivity ρ increases exponentially with temperature:

$$\rho \sim e^{e\varphi_s/kT} \tag{24}$$

By application of an external voltage V the barrier $E \equiv e\varphi_S(0)$ is reduced and the resistivity ρ changes accordingly.

$$\varphi_s(V) = \varphi_s(0)\left(1 - \frac{V}{4\varphi_s}\right) \tag{25}$$

The varistor effect

Usually current/voltage curves of varistors (fig.16) are fitted by

$$I \sim V^{\alpha} \qquad \left(\alpha = \frac{V}{I}\frac{dI}{dV}\right) \tag{26}$$

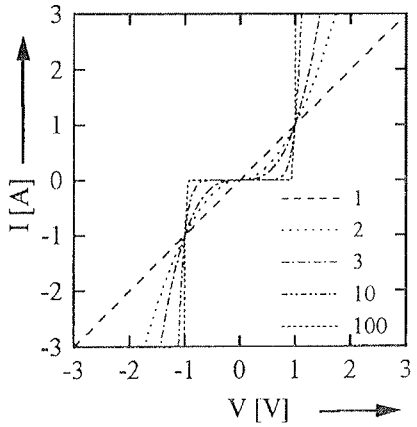

Fig.16: Schematic current/voltage curves, taken from /16/

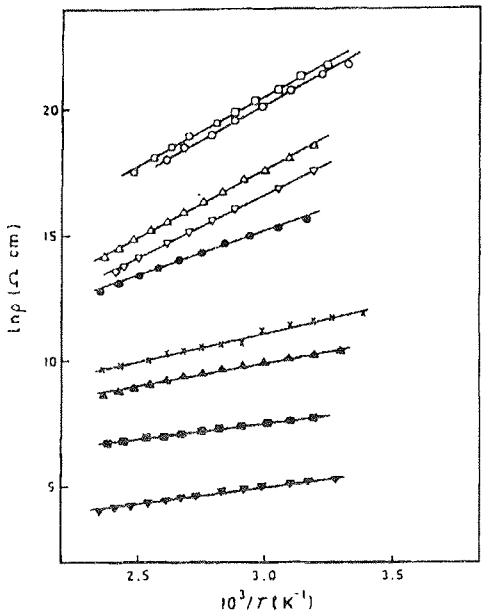

Fig. 17: DC resistivities of a differently quenched ZnO varistor

An example for a double Schottky layer evaluation is taken from /17/. In fig.17 and 18 DC resitivities vs. temperature and CV plots are reproduced. According to equ. (24) from the slope of resitivity at low voltages the barrier height is found to be of the order of 0.5 eV, but depends strongly on the quenching temperature. Reciprocal CV plots according to equ.(19) give straight lines, from which donor and acceptor densities can be obtained.

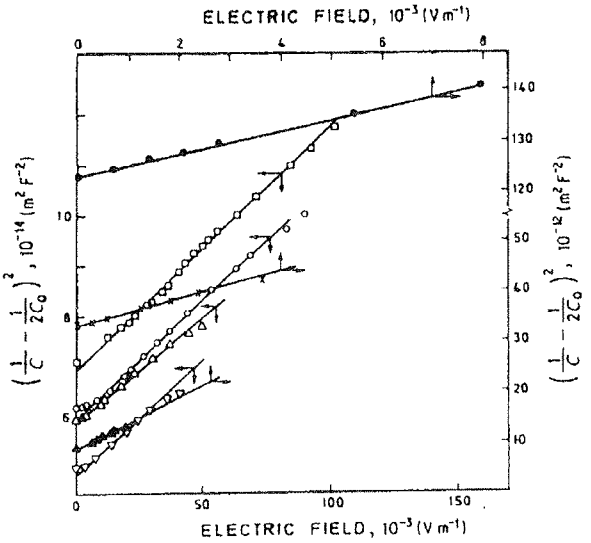

Fig. 18: Schottky plot of a differently quenched ZnO varistor (C capacitance; C_0 zero field capacitance)

Results of the evaluation are plotted in fig.19. At processing temperatures higher than about 800 °C defect equilibrium and barrier formation seem to be established.

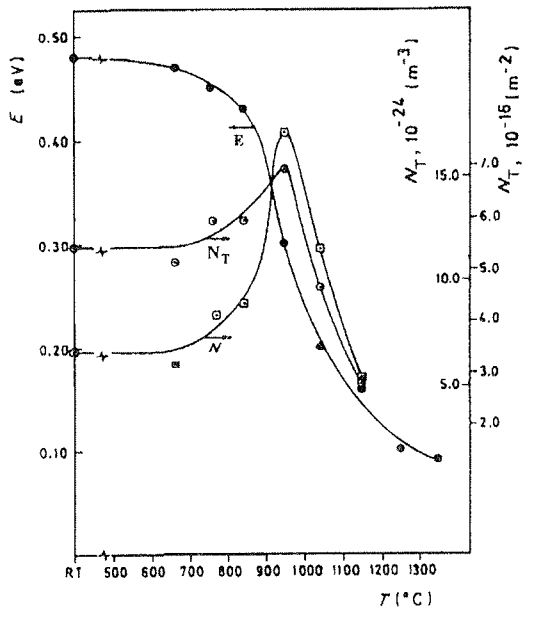

Fig.19: Dependence of activation energy E, donor density N and trap density N_T on quenching temperature

The dielectrical breakdown of ZnO varistors begins beyond 3.2 V per grain boundary, which is equal to the band gap energy. For the steep current increase a lot of different tunnelling models have been proposed (fig. 20) /18/. For the explanation of the extremely non-linear current the minority carriers in combination with ionic lattice defects seem to play an essential role. A lot of work on chemical tailoring of varistors, beginning with Matsuoka /19/ has been done especially by Kolar et al. /20/.

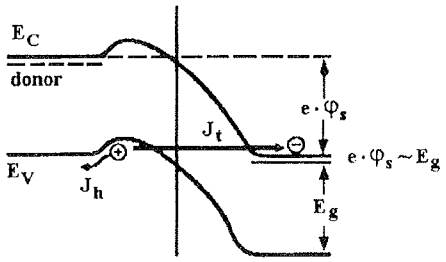

Fig. 20: Zener band to band tunneling, taken from /16/

The PTC effect

The PTC characteristics, i.e. DC-resistivity of about 10Ωcm below and about 6-8 orders, of magnitude higher above the Curie temperature, is easily understood from equ.(23-25). Below the Curie temperature the dielectric constant of $BaTiO_3$ is by a factor of about 100 greater and the barrier height lower than above. Thus the PTC characteristics is not only a space charge effect, but coupled to the ferroelectric property of the base material $BaTiO_3$. Without donor doping $BaTiO_3$ would behave as a capacitor, which is also widely used in electroceramics. As with all electroceramic components, PTC processing is made at high temperature, so

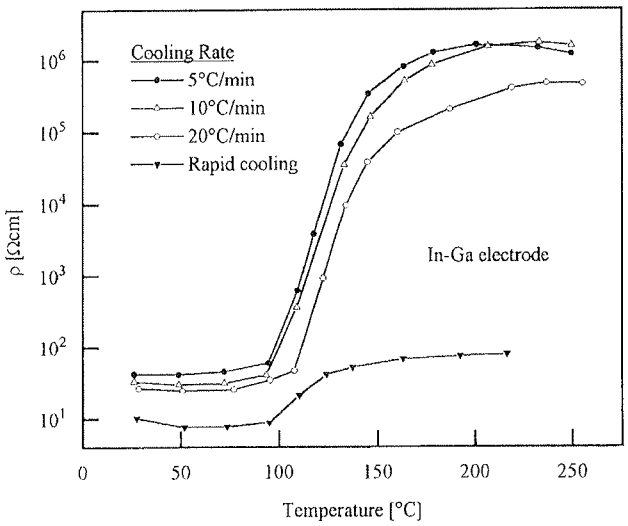

Fig. 21: PTC effect for different cooling rates /21/

that sintering temperature, soaking time, cooling rate etc. influence dramatically the formation of the barrier layers at the grain boundaries (fig. 21).

From impedance measurements the following simple equivalent circuit consisting of an ohmic bulk resistance, a grain boundary and an electrode interface impedance is proposed (fig. 22).

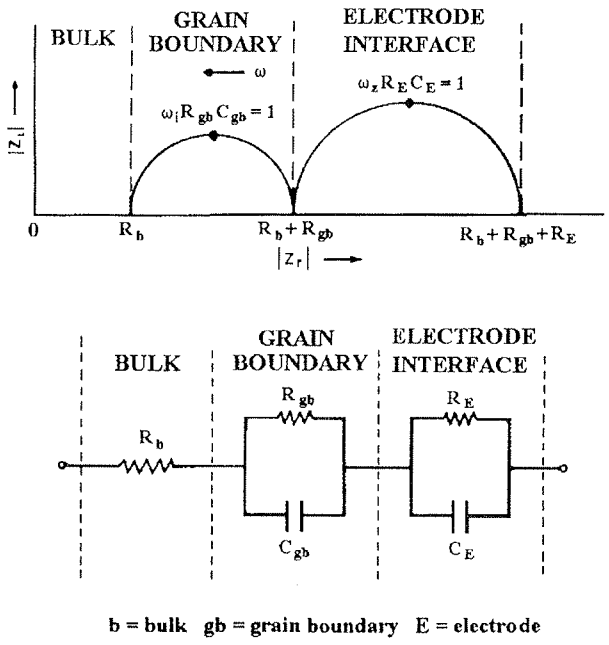

Fig. 22: Generalised impedance diagram and equivalent circuit /21/

Passive Layers

Ionic space charges within passivating layers may play an important role for the mass transport e.g. in Li-batteries. Nowadays great effort is made to develop layered batteries. The key to more progress in this technology seems to be the nature of the passive layer between metallic Li and the electrolyte, which roughly can be compared with a polycrystalline ceramic layer.

Li-$SOCl_2$ ($AlCl_3$) contacts have been extensively studied by Pejovnik and coworkers /22/. The as-grown LiCl layer behaves like a good Li^+ conductor, at least because of Al^{+++} doping during passivation and growth. A space charge at the metal contact is assumed to be built up by depleted mobile Li^+ and enhanced immobile Cl^- vacancies, being responsible for the high ohmic resistance. When anodically biased, the depletion and the enhancement are lowered and the resistance decreases (fig. 23). As the accomodation of the space charge region needs some time, battery charging is delayed.

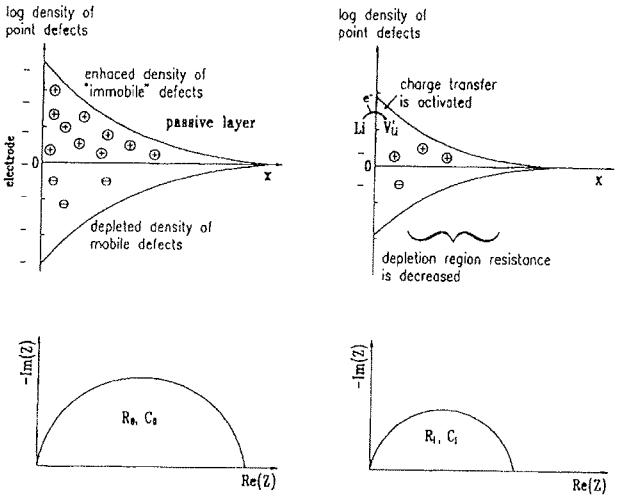

Fig. 23: Space charge model for Li-passive layer without and with bias, taken from /22/

IV. SPACE CHARGES AT PHOTOACTIVE MATERIALS

Aspects of usefulness of space charges are to be considered, when a semiconductor interface is irradiated with light of band gap wavelength. The light will excite electrons from the valence to the conduction band, thus creating electron-hole pairs. After dissociation and some time of diffusion the charge carriers will combine radiationless. However, if this creation of holes happens within a region of high stationary electrical field, the pairs will be separated to give an electron and a hole current, in other words to give a photo current /23/. This photo current can be used in a positive practical sense in photo devices, but is awful when it leads to progressive corrosion or destruction of the semiconducting material /24/.

The sources of high electric fields are once again space charges, created at semiconductor interfaces. External biasing increases or lowers the space charge and thus the field. In the following the photo effect of some solar devices is qualitatively explained.

Dry Solar Cells

As shown in fig. 24 at a metal-n semiconductor-metal structure in the dark there is a certain band bending and electric field on both sides of the semiconductor. If one metal side is made transparent and illuminated with light of band gap, positive holes will flow to the negative charged metal and electrons to the opposite side. Thus a discharge of the illuminated space charge is obtained. At constant illumination a steady state will be reached, when in the decreasing field the production of electron-hole pairs is balanced by their recombination. In this non equilibrium steady state a difference of the metal Fermi levels arises, which is equivalent to a photo emf. If the

external circuit contains a consumer, a photo current is observed. The same principle holds for Si pn-contacts, today being the most interesting commercial solar device.

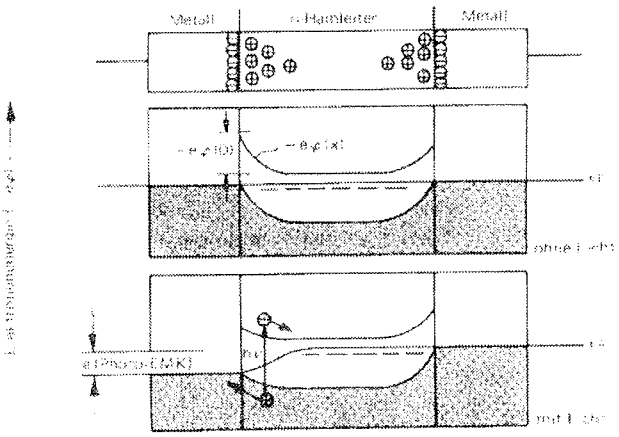

Fig. 24: Photo effect at a metal-semiconductor contact /1/

Electrolytical Solar Cells

Quite similar electron-hole pairs are generated in an electrolytical solar cell, which can be in combination with a counter electrode to give a solar battery. The basic component is a transparent semiconductor-electrolyte contact, whose diffuse space charge is able to separate photo electrons from holes (fig. 25).

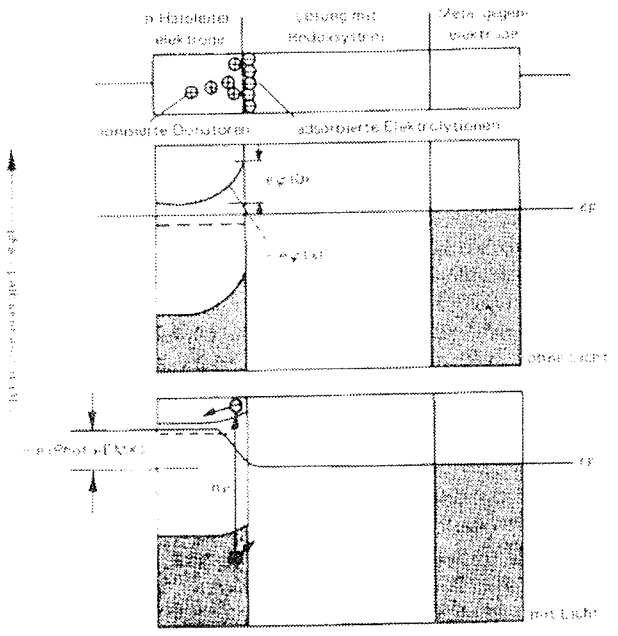

Fig. 25: Photo effect at a semiconductor-electrolyte contact /1/

However, instead of an external bias to create a space charge, the latter is here performed by an internal redox system. Under open circuit conditions the according Nernst potential is established and if this one is positive enough, a Schottky depletion layer will be formed. On illumination discharge and a photo emf will occur. If there are enough hole acceptors present in the electrolyte, and if there are corresponding reactions at the counter electrode possible, the device can act as a battery.

In the past one tried to construct regenerative and energy storing batteries, but two serious disadvantages prevented from a commercial application. Reasonable semiconductor electrodes were made of oxides or sulfides and these materials are 1. to a certain extent soluble in the electrolyte and 2. oxidable by the holes itself. Thus lattice anions are oxidised and the material decomposes.

Photo catalysis

Photo hole and electron production with subsequent reactions can be utilized in some chemical devices and for instance considered for waste water treatment. The degradation of organic material in waste water can be enhanced effectfully by suspending and illuminating TiO_2 powder within the band gap. A flux of oxidising holes and reducing electrons at the oxide surface will be the result of the illumination, so that one can speak of a catalytical photo effect.

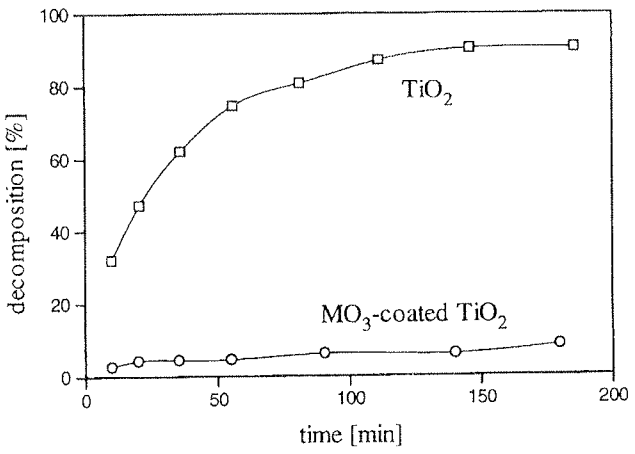

Fig. 26: Photo catalytical decomposition of dichlorpyridine into CO_2 in illuminated suspensions of MO_3- coated (o) and uncoated (□) TiO_2 powders /25/

References

/1/ G.M. Barrow, G.W. Herzog: Physikalische Chemie, Bohmann-Vieweg, Wien-Wiesbaden,1984,.

/2/ G. Achatz, J. Friedman, G.W.Herzog: Surf. Techn.6(1978) 455

/3/ G. Achatz, O. Fruhwirth, G.W. Herzog, W. Plot: Surf. Techn. 9(1979) 323

/4/ G.W. Herzog, H. Leitner: Surf. Coat. Techn.27(1986) 29

/5/ D.J. Adams, Molec. Phys.29(1975) 307

/6/ G. Ertl, H. Gerischer: in Physical Chemistry, eds. Eyring, Henderson, Jost, Volume X, Acad. Press. N.Y.,1970

/7/ J. Friedman, O. Fruhwirth, G.W. Herzog: Surf. Techn.6(1978) 469

/8/ De Witt G. Ong: Modern MOS Technology, McGraw-Hill N.Y. 1984

/9/ V.L. Rideout, F. H. Gaerssien, A. LeBlanc: IBM J. Res. Develop. 1975

/10/ K. Ziegler, E. Klausmann, S. Kar: Solid State Electronics 18(1975) 189

/11/ O. Fruhwirth, G.W. Herzog: Unpublished Report for Siemens Villach 1987

/12/ A. Goetzberger, E. Klausmann, M.J. Schulz: Crit. Rev. Solid State Phys.6(1976) 1

/13/ W.A. Tiller: J. Electrochem. Soc.127(1980) 625

/14/ B.E. Deal: Trans. Electron. Devices,27(1980) 1380

/15/ G. Mader, H. Meixner, P. Kleinschmidt: Siemens F&E Ber. 16(1987) 76

/16/ R. Einzinger: Ann. Rev. Mater. Sci.17(1987) 299

/17/ P.Q. Mantas, A.M.R. Senos, J.L. Baptista: J. Mater. Sci. 21(1986) 679

/18/ L.M. Levinson, H.R. Philipp: J. Appl. Phys.46(1975) 1332

/19/ M. Matsuoka: Jpn. J. Appl. Phys.10(1971) 736

/20/ M. Trontelj, D. Kolar, V. Kraševec: Mater. Sci. Res.20(1986) 509

/21/ R.N. Basu, H.S. Maiti: High Tech Ceramics, ed. P.Vincenzini, Elsevier Sci. Publ., Amsterdam 1985

/22/ M. Gaberšček, J. Jamnik, S. Pejovnik: J. Power Sources 43-44(1993) 391

/23/ V. Myamlin, Y. V. Pleskov: Electrochemistry of Semiconductors, Plenum Press, N.Y.1967

/24/ S.R. Morrison, T. Freund: Electrochim. Acta 13(1968) 1843

/25/ J. Poulios: University of Thessaloniki, private communication 1995

Dr. Gerhard Herzog, dipl.ing.,
Institut für Chemische Technologie
Anorganischer Stoffe
Technische Universität Graz,
A-8010 Graz, Stremayrgasse 16
Tel.: +43 316 873 82 85
Fax: + 43 316 83 76 19

Prispelo (Arrived): 28.09.1995 *Sprejeto (Accepted): 07.11.1995*